Inorganic Chemistry

ARTICLE

pubs.acs.org/IC

Tetradentate vs Pentadentate Coordination in Copper(II) Complexes of Pyridylbis(aminophenol) Ligands Depends on Nucleophilicity of Phenol Donors

Rajendra Shakya,[†] Zhaodong Wang, Douglas R. Powell, and Robert P. Houser*

Department of Chemistry and Biochemistry, University of Oklahoma, 101 Stephenson Parkway, Norman, Oklahoma 73019-5251, United States

Supporting Information

ABSTRACT: The ligand binding preferences of a series of potentially pentadentate pyridylbis(aminophenol) ligands were explored. In addition to the previously reported ligands 2,2′-(2-methyl-2-(pyridin-2-yl)propane-1,3-diyl)bis(azanediyl)bis(methylene)-diphenol (H_2L^1) and 6,6′-(2-methyl-2-(pyridin-2-yl)propane-1,3-diyl)bis(azanediyl)bis(methylene)bis(2,4-di-*tert*-butylphenol) ($H_2L^{1\text{-}tBu}$), four new ligands were synthesized: 6,6′-(2-methyl-2(pyridine-2-yl)propane-1,3-diyl)bis(azanediyl)bis(methylene)bis-(2,4-dibromophenol) ($H_2L^{1\text{-}Br}$), 6,6′-(2-methyl-2(pyridine-2-yl)propane-1,3diyl)bis(azanediyl)-bis(methylene)bis(2-methoxyphenol) ($H_2L^{1\text{-}MeO}$), 2,2′-(2-methyl-2(pyridine-2-yl)propane-1,3diyl)bis(azanediyl)bis(methylene)bis(4-nitrophenol) ($H_2L^{1\text{-}NO2}$), and 2,2′-(2-phenylpropane-1,3-diyl)bis(azanediyl)bis(methylene)diphenol (H_2L^2). These ligands, when combined with copper(II) salts and base, form either tricopper(II) species or monocopper(II) species depending on the nucleophilicity of the phenol groups in the ligands. All copper complexes were characterized by X-ray crystallography, cyclic voltammetry, and spectroscopic methods in solution. The ligands in trimeric complexes $[\{CuL^1(CH_3CN)\}_2Cu](ClO_4)_2$ (**1**), $[\{CuL^1Cl\}_2Cu]$ (**1a**), and $[\{CuL^2(CH_3CN)\}_2Cu](ClO_4)_2$ (**1b**) and monomeric complex $[CuL^{1\text{-}tBu}(CH_3OH)]$ (**2**) coordinate in a tetradentate mode via the amine N atoms and the phenolato O atoms. The pyridyl groups in **1**, **1a**, and **2** do not coordinate, but instead are involved in hydrogen bonding. Monomeric complexes $[CuL^{1\text{-}Br}]$ (**3a**), $[CuL^{1\text{-}NO2}]$ (**3b**), and $[CuL^{1\text{-}MeO}Na(CH_3OH)_2]ClO_4$ (**3c**) have their ligands coordinated in a pentadentate mode via the amine N atoms, the phenolato O atoms, and the pyridyl N atom. The differences in tetradentate vs pentadentate coordination preferences of the ligands correlate to the nucleophilicity of the phenolate donor groups, and coincide with the electrochemical trends for these complexes.

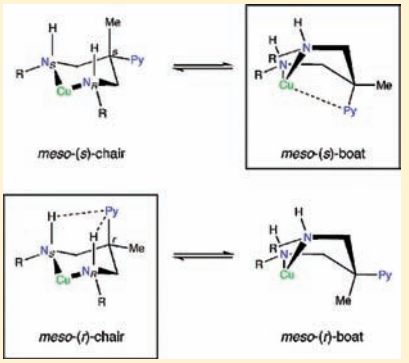

INTRODUCTION

Polydentate ligands serve myriad purposes in coordination chemistry. Important progress in inorganic chemistry, far too voluminous to enumerate here, has been made at least in part because of control over structure and reactivity imparted by polydentate ligands. Polydentate ligands can coordinate to different metal ions with varying denticity depending on the coordination number and geometry preferences of the metal. This principle of "maximum site occupancy", where coordinatively saturated complexes are formed with all ligand binding sites being used, was recently exploited to form heteronuclear complexes.[1] However, it is not uncommon for polydentate ligands to coordinate via fewer than all of their ligand binding sites. Ambiguous coordination possibilities for polydentate ligands in naming inorganic complexes are resolved by the IUPAC nomenclature standards and rules.[2] Different coordination preferences of different metal ions can lead to varying denticity, as exemplified by a *N,N*-bis(2-picolyl)amine derivative with a pendant ethoxyethanol side chain.[3] This ligand coordinates with κ^5 denticity with Co(II), Ni(II), and Zn(II), but with reduced denticity (κ^4 or κ^3, depending on whether a long axial Cu−O interaction is interpreted as a bond or not) with Cu(II) because of the expected Jahn−Teller distortion.[3] This situation can also result from steric constraints that prevent the ligand from coordinating via all donor atoms. For example, Cu(II) complexes from our laboratory using pyridylbis(imine) or pyridylbis(guanidine) ligands coordinate such that the pyridyl ring is spatially too far from the metal center to coordinate.[4] Similarly, Fe(II) complexes of a tetradentate 1,2-dipyridyl-1,2-diaminoethane ligand display κ^3 denticity because of steric constraints.[5] Finally, modifications to the ligand can lead to changes in denticity. An example of this was reported where a cyclam ligand goes from κ^4 to κ^3 in a Ru(III) nitrosyl complex when one of the N-atoms of the cyclam was substituted with a carboxypropyl pendant arm.[6] While the authors did not definitively pinpoint the reason for the change in denticity, they offer some possible explanations ranging from the reduced σ-donor ability of the N-atom, to steric and kinetic arguments.[6] Here we describe another example of a ligand system that displays variable denticity that we believe is electronically based.

Previously we reported a new family of ligands based on the pyridylbis(acetamide) ligand, $H_2pp(ac)_2$,[7] that contain phenol

Received: July 19, 2011
Published: October 18, 2011

Scheme 1

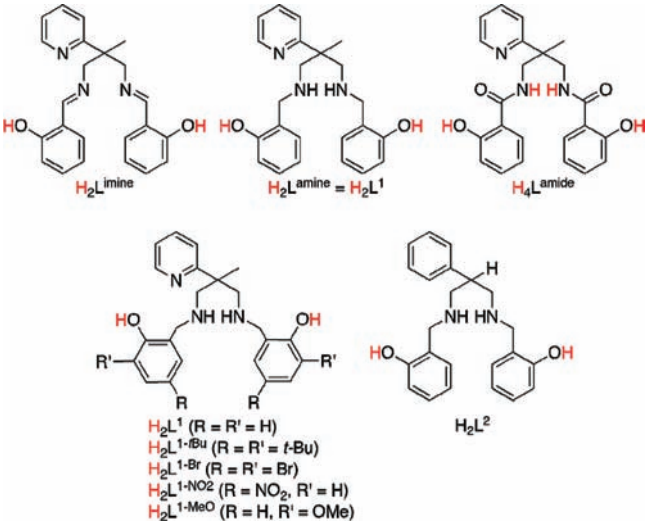

groups appended to the nitrogens.[4a] While not the focus of the present work, copper coordination chemistry with phenol-containing ligands continues to attract attention because of its relevance to galactose oxidase.[8] The ligands included a pyridylbis(amidophenol), H_4L^{amide}, a pyridylbis(iminophenol), H_2L^{imine}, and a pyridylbis(aminophenol), H_2L^{amine} (Scheme 1). The structures of the copper(II) complexes that formed were dependent on the nature of the ligands. The copper(II) complexes that were isolated and characterized had varying nuclearity ranging from mononuclear $[Cu(L^{imine})(CH_3OH)]$, to trinuclear $[\{CuL^{amine}(CH_3CN)\}_2Cu]$, to hexanuclear $[Cu_6(HL^{amide})_4(H_2O)_2]$.[4a] H_2L^{imine} forms a monomeric species, $[Cu(L^{imine})(CH_3OH)]$, where the ligand has been deprotonated at the phenol O positions, making the ligand dianionic. The amide ligand H_4L^{amide} forms a hexacopper cluster, $[Cu_6(HL^{amide})_4(H_2O)_2]$, where each ligand has had three protons removed to form a trianionic ligand. Finally, H_2L^{amine} forms a tricopper complex, $[\{CuL^{amine}(CH_3CN)\}_2Cu]$ (**1**). Using the amine ligand H_2L^{amine} and its *tert*-butyl substituted derivative $H_2L^{tBu\text{-}amine}$ we similarly explored the iron(III) chemistry of these ligands.[9]

The amine ligand H_2L^{amine}, henceforth in this paper referred to as H_2L^1, coordinates to the copper ions in **1** in a tetradentate fashion where the pyridyl ring was not coordinated to the copper center. However, in the iron(III) complexes of H_2L^1 and $H_2L^{tBu\text{-}amine}$ (henceforth referred to as $H_2L^{1\text{-}tBu}$), the pyridyl ring does coordinate, rendering the ligands pentadentate chelators. Seeking to understand why H_2L^1 and $H_2L^{1\text{-}tBu}$ act as a tetradentate ligand in some instances and a pentadentate ligand in others, we set out to expand the copper(II) coordination chemistry of the pyridylbis(aminophenol) ligands. Here we report three new ligands in the H_2L^1 family of pyridylbis(aminophenol) ligands, their copper(II) coordination chemistry, and provide insight into the tetradentate versus pentadentate chelating preferences of these ligands on the basis of the nucleophilicity of the phenol rings.

EXPERIMENTAL SECTION

General Procedures. Unless otherwise stated, all reagents were used as received from commercial sources. 2-methyl-2-(pyridine-2-yl) propane-1,3-diamine (ppda),[10] 2,2′-(2-methyl-2-(pyridin-2-yl)propane-1,3-diyl)bis(azanediyl)bis(methylene)diphenol (H_2L^1),[4a] and 6,6′-(2-methyl-2-(pyridin-2-yl)propane-1,3-diyl)bis(azanediyl)bis(methylene)-bis(2,4-di-*tert*-butylphenol) ($H_2L^{1\text{-}tBu}$)[9] were synthesized according to published procedures. 2-Phenylpropane-1,3-diamine (phpda)[11] was synthesized according to a modified procedure, following the method used for ppda. Solvents used were doubly purified using alumina columns in a MBraun solvent purification system (MB-SPS). Infrared spectra were measured from 4000 to 400 cm^{-1} as KBr pellets on a NEXUS 470 FTIR spectrometer. ^1H NMR spectra were measured using a Varian 300 MHz instrument. Mass spectra were measured on a Q-TOF quadrupole time-of-flight mass spectrometer (Micromass, Manchester, U.K.) equipped with a Z-spray electrospray ionization (ESI) source. Elemental analyses were performed by Atlantic Microlab, Norcross, GA. UV−visible spectra were measured using a Shimadzu UV2401PC spectrophotometer in the range 250 to 1000 nm on solutions ranging in concentration from 1.0×10^{-3} M and 1.0×10^{-4} M. Cyclic voltammetry experiments were performed using a BAS 50W potentiometer and a standard three-electrode cell with a glassy-carbon working electrode, a Pt-wire auxiliary electrode, and an Ag/AgCl reference electrode under an inert atmosphere at room temperature. X-band EPR spectra of the complexes were recorded at 77 K using a Bruker EMX spectrometer. Magnetic susceptibilities of the complexes in the solid state were measured at 295 K using a Johnson Matthey magnetic susceptibility balance (MSB−AUTO) with a magnetic field strength of 4.5 kGauss and a measurement range of $\pm 1.999 \times 10^{-4}$ to $\pm 5 \times 10^{-10}$ cgs. Solution magnetic susceptibilities were measured at 295 K by the Evans method.[12]

Synthesis of $H_2L^{1\text{-}Br}$, $H_2L^{1\text{-}NO2}$, and $H_2L^{1\text{-}MeO}$. The ligands $H_2L^{1\text{-}Br}$, $H_2L^{1\text{-}NO2}$, and $H_2L^{1\text{-}MeO}$ were prepared by the same general procedure in which ppda (0.330 g, 2.00 mmol) was condensed with the appropriate aldehyde (4.00 mmol) in 40 mL of methanol at 50 °C. After 2 h, $NaBH_4$ (0.220 g, 6.00 mmol) was added into the solution in small portions at 0 °C. The solution was then stirred at room temperature for 2 h, the solvent was evaporated, and the amine product was extracted with dichloromethane, dried over anhydrous $MgSO_4$, and isolated after solvent evaporation.

6,6′-(2-Methyl-2(pyridine-2-yl)propane-1,3-diyl)bis(azanediyl)bis(methylene)bis(2,4-dibromophenol) ($H_2L^{1\text{-}Br}$). 3,5-Dibromosalicylaldehyde (1.12 g, 4.00 mmol) was the aldehyde used in the synthesis of $H_2L^{1\text{-}Br}$ (0.826 g, 60% yield). Anal. Calcd for $C_{23}H_{23}Br_4N_3O_2$: C, 39.9; H, 3.3; N, 6.1. Found: C, 40.4; H, 3.4; N, 5.8. ^1H NMR (300 MHz, CD_2Cl_2, 300 K) δ 1.46 (s, 3H), 2.91 (d, J = 12 Hz, 2H), 3.06 (d, J = 11.7 Hz, 2H), 3.40 (d, J = 14.4 Hz, 2H), 3.98 (d, J = 14.4 Hz, 2H), 7.10−7.34 (m, 4H), 7.53−7.75 (m, 3H), 8.52 (d, J = 9 Hz, 1H) ppm. FTIR (KBr): 3288 (O−H), 3071 (s), 2842 (s), 1589, 1569, 1454 (s), 1384, 1282, 1260, 1152, 1089, 993, 860, 787, 748, 684, 651 cm^{-1}. ESI-MS (MeOH): m/z = 693 $[H_2L^{1\text{-}Br} + H]^+$.

2,2′-(2-Methyl-2(pyridine-2-yl)propane-1,3diyl)bis(azanediyl)-bis(methylene)bis(4-nitrophenol) ($H_2L^{1\text{-}NO2}$). 2-Hydroxy-5-nitrobenzaldehyde (0.668 g, 4.00 mmol) was the aldehyde used in the synthesis of $H_2L^{1\text{-}NO2}$ (0.654 g, 70% yield). Anal. Calcd for $C_{23}H_{25}N_5O_6 \cdot 2CH_3OH$: C, 56.5; H, 6.3; N, 13.2. Found: C, 56.1; H, 5.5; N, 12.6. ^1H NMR (300 MHz, CD_2Cl_2, 300 K) δ 1.45 (s, 3H), 2.99 (d, J = 12 Hz, 2H), 3.14 (d, J = 11.7 Hz, 2H), 3.43 (s, 2H), 3.73 (s, 2H), 4.00 (m, 4H), 6.83 (d, J = 4.2 Hz, 1H); 7.24−7.37 (m, 4H), 7.78−8.08 (m, 3H), 8.53 (d, J = 9.0 Hz, 1H) ppm. FTIR (KBr): 3431 (O−H), 2930 (s), 1593, 1476 (s), 1335, 1284, 1157, 1089, 995, 865, 787, 752, 650 cm^{-1}. ESI-MS (MeOH): m/z = 468 $[H_2L^{1\text{-}NO2} + H]^+$.

6,6′-(2-Methyl-2(pyridine-2-yl)propane-1,3diyl)bis(azanediyl)bis(methylene)bis(2-methoxyphenol) ($H_2L^{1\text{-}MeO}$). 2-Hydroxy-3-methoxybenzaldehyde (0.608 g, 4.00 mmol) was the aldehyde used in the synthesis of $H_2L^{1\text{-}MeO}$ (0.570 g, 65% yield). Anal. Calcd for $C_{25}H_{31}N_3O_4 \cdot H_2O$: C, 65.9; H, 7.3; N, 9.2. Found: C, 65.6; H, 7.2; N, 8.9. ^1H NMR (300 MHz, $CDCl_3$, 300 K) δ 1.49

(s, 3H), 2.88 (d, J = 11.4 Hz, 2H), 3.14 (d, J = 11.7 Hz, 2H), 3.82 (s, 6H), 3.90 (m, 4H), 6.58−6.78 (m, 6H), 7.13−7.64 (m, 3H), 8.50 (d, J = 6 Hz, 1H) ppm. FTIR (KBr): 3418 (O−H), 2832 (s), 1589, 1477 (s), 1328, 1232, 1158, 1074, 769, 732, 621 cm^{-1}. ESI-MS (MeOH): m/z = 438 $[H_2L^{1\text{-MeO}} + H]^+$.

Syntheses of 2,2′-(2-Phenylpropane-1,3-diyl)bis(azanediyl)-bis(methylene)diphenol (H_2L^2). The ligand H_2L^2 was prepared by the condensation of phpda (0.375 g, 2.50 mmol) with salicylaldehyde (0.610 g, 5.00 mmol) in a 25 mL MeOH solution. The solution was stirred at 50 °C for 2 h, yielding a pale yellow solution. $NaBH_4$ (0.285 g, 7.50 mmol) was then added at 0 °C in small portions. The solution was stirred at room temperature for 2 h, the solvent was evaporated, and the product amine was extracted with dichloromethane, dried over $MgSO_4$, and isolated after solvent evaporation (0.68 g, 75% yield). Anal. Calcd for $C_{23}H_{26}N_2O_2 \cdot {}^1/_2CH_3OH$: C, 74.6; H, 7.5; N, 7.4. Found: C, 75.1; H, 7.2; N, 7.1. ^1H NMR (300 MHz, $CDCl_3$, 293 K) δ 2.78−2.92 (m, 4H), 3.02−3.08 (m, 1H), 3.78−3.89 (m, 4H), 6.65−6.74 (m, 4H), 6.85−6.88 (m, 2H), 7.05−7.30 (m, 7H) ppm. FTIR (KBr): 3295 (O−H), 3027−2842 (s), 1615 (s), 1588 (s), 1490 (s), 1458 (s), 1255, 1182, 1151, 1102, 1034, 971, 932, 844, 753, 720, 700, 617, 540, 451 cm^{-1}. ESI-MS (MeOH): m/z = 363 $[H_2L^2 + H]^+$.

Syntheses of the Complexes. A general synthetic route was used for the preparation of all complexes in which, under an open air atmosphere, the appropriate Cu(II) salt was added to a solution of the respective ligand (0.100 mmol) in acetonitrile for **1b** and in methanol for **1a**, **2**, and **3a**−**c**. For complexes **1a**−**b**, **2**, and **3a**−**b**, Et_3N (0.040 mL, 0.30 mmol) was used as the base for phenol deprotonation. For **3c**, NaH (0.072 g, 0.30 mmol) was used as the base for phenol deprotonation. In each case, the resulting dark green solution was stirred for 2 h at room temperature and filtered to remove any unreacted solids. X-ray quality crystals of all complexes were obtained after crystallization by appropriate methods.

Caution! *Perchlorate salts of metal complexes with organic ligands are potentially explosive. Although no difficulty was encountered during the syntheses described herein, they should be prepared in small amounts and handled with caution.*

[{CuL^{1}Cl}$_2$Cu] (1a). H_2L^1 (0.037 g, 0.10 mmol) and $CuCl_2 \cdot 2H_2O$ (0.017 g, 0.10 mmol) were used (0.031 g, 60% yield). Anal. Calcd for $C_{46}H_{50}Cl_2Cu_3N_6O_4$: C, 54.6; H, 5.0; N 8.3. Found: C, 54.8; H, 5.3; N, 8.2. UV/vis (CH_2Cl_2) [λ_{max}, nm (ε, M^{-1} cm^{-1})]: 335 (39,000), 396 (3,240), 645 (450 sh). FTIR (KBr): 1597 (s), 1577 (s) 1487, 1456, 1400, 1274, 1261, 1201, 1114, 1042, 995, 875, 787, 751, 732, 605, 467, 413 cm^{-1}. ESI-MS (MeOH): m/z = 439 $[CuL^1 + H]^+$, 974 $[Cu_3(L^1)_2Cl]^+$. EPR (9.436 GHz, mod. amp. 5.0 G, CH_2Cl_2, 77 K): $g_\parallel$ = 2.233, $g_\perp$ = 2.025, and $A_\parallel$ = 186 G. Solution magnetic moment (Evans method, 19.8 °C, 6.67 × 10^{-3} M, chloroform-d_1): 1.09 μ_B/Cu. Solid state magnetic moment (MSB-Auto, 4.5 kG, 22.0 °C): 1.00 μ_B/Cu.

[{CuL^2(CH$_3$CN)}$_2$Cu](ClO$_4$)$_2$ (1b). H_2L^2 (0.036 g, 0.10 mmol) and $Cu(ClO_4)_2 \cdot 6H_2O$ (0.037 g, 0.10 mmol) were used (0.036 g, 65% yield). The sample for elemental analysis was powdered and dried under vacuum overnight, removing acetonitrile solvent of crystallization from the complex. However, the complex being hygroscopic, a water molecule was found to be associated in its elemental analysis. Anal. Calcd for $C_{46}H_{48}Cl_2Cu_3N_4O_{12} \cdot H_2O$: C, 49.0; H, 4.5; N 5.0. Found: C, 48.7; H, 4.5; N, 5.0. UV/vis (CH_3CN) [λ_{max}, nm (ε, M^{-1} cm^{-1})]: 285 (27,300), 392 (3,070), 592 (450 sh). FTIR (KBr): 1599 (s), 1578, 1487 (s), 1457 (s) 1400, 1274, 1254, 1203, 1117, 1098, 1087 (ClO_4^-), 995, 875, 763, 703, 624, 602, 535, 469, 415 cm^{-1}. ESI-MS (MeOH): m/z = 455 $[Cu_3(L^2)_2]^{2+}$. EPR (9.444 GHz, mod. amp. 10.0 G, CH_3CN, 77 K): $g_\parallel$ = 2.28, $g_\perp$ = 2.07, and $A_\parallel$ = 160 G. Solution magnetic moment (Evans method, 19.8 °C, 5.50 × 10^{-3} M, acetonitrile-d_3): 1.11 μ_B/Cu. Solid state magnetic moment (MSB-Auto, 4.5 kG, 22.0 °C): 0.940 μ_B/Cu.

[CuL$^{1\text{-}t\text{Bu}}$(CH$_3$OH)] (2). $H_2L^{1\text{-}t\text{Bu}}$ (0.060 g, 0.10 mmol) and $Cu(ClO_4)_2 \cdot 6H_2O$ (0.037 g, 0.10 mmol) were used (0.046 g, 70% yield). Anal. Calcd for $C_{40}H_{61}CuN_3O_3$: C, 69.1, H, 8.8, N 6.0. Found: C, 68.6, H, 8.8, N, 6.2. UV/vis (CH_2Cl_2) [λ_{max}, nm (ε, M^{-1} cm^{-1})]: 298 (11,200), 406 (1,600), 597 (855). FTIR (KBr): 2950−2865 (s), 1617 (s), 1592 (s), 1528, 1471 (s), 1437 (s), 1413, 1384, 1304, 1273, 1202, 1169, 1063, 830, 790, 748, 480 cm^{-1}. ESI-MS (MeOH): m/z = 663 $[CuL^{1\text{-}t\text{Bu}} + H]^+$. EPR (9.432 GHz, mod. amp. 5.0 G, CH_2Cl_2, 77 K): $g_\parallel$ = 2.225, $g_\perp$ = 1.998, and $A_\parallel$ = 184 G. Solution magnetic moment (Evans method, 19.8 °C, 5.50 × 10^{-3} M, acetonitrile-d_3): 1.70 μ_B/Cu. Solid state magnetic moment (MSB-Auto, 4.5 kG, 22.0 °C): 1.50 μ_B/Cu.

[CuL$^{1\text{-Br}}$] (3a). $H_2L^{1\text{-Br}}$ (0.0693 g, 0.100 mmol) and $Cu(OTf)_2$ (0.036 g, 0.10 mmol) were used (0.0527 g, 65% yield). Anal. Calcd for $C_{23}H_{21}Br_4CuN_3O_2 \cdot {}^1/_2CH_2Cl_2$: C, 35.4, H, 2.8, N 5.3. Found: C, 35.3, H, 2.6, N, 5.4. UV/vis (CH_2Cl_2) [λ_{max}, nm (ε, M^{-1} cm^{-1})]: 306 (10,300), 352 (2,800), 407 (2,380), 648 (180). FTIR (KBr): 3107 (s), 2919 (s), 2361, 2338, 1652, 1575, 1434 (s), 1398, 1300, 1264, 1155, 1090, 1035, 860, 789, 750, 667, 627 cm^{-1}. ESI-MS (MeOH): m/z = 776 $[CuL^{1\text{-Br}} + Na]^+$. EPR (9.442 GHz, mod. amp. 10.0 G, DMSO, 77 K): $g_\parallel$ = 2.350, $g_\perp$ = 2.109, and $A_\parallel$ = 169 G. Solution magnetic moment (Evans method, 19.8 °C, 5.50 × 10^{-3} M, chloroform-d_1): 1.73 μ_B/Cu. Solid state magnetic moment (MSB-Auto, 4.5 kG, 22.0 °C): 1.60 μ_B/Cu.

[CuL$^{1\text{-NO2}}$] (3b). $H_2L^{1\text{-NO2}}$ (0.0467 g, 0.100 mmol) and $Cu(ClO_4)_2 \cdot 6H_2O$ (0.0370 g, 0.100 mmol) were used (0.0339 g, 60% yield). Anal. Calcd for $C_{23}H_{23}CuN_5O_6 \cdot 2H_2O$: C, 48.9, H, 4.8, N 12.4. Found: C, 48.7, H, 4.8, N, 12.4. UV/vis (CH_3CN) [λ_{max}, nm (ε, M^{-1} cm^{-1})]: 404 (29,400), 641 (290 sh). FTIR (KBr): 3164 (s), 1652, 1596, 1479 (s), 1437, 1399, 1290, 1182, 1092, 928, 898, 835, 760, 667 cm^{-1}. ESI-MS (MeOH): m/z = 529 $[CuL^{1\text{-NO2}} + H]^+$. EPR (9.449 GHz, mod. amp. 4.0 G, DMSO, 77 K): $g_\parallel$ = 2.316, $g_\perp$ = 2.10, and $A_\parallel$ = 176 G. Solution magnetic moment (Evans method, 19.8 °C, 5.50 × 10^{-3} M, dimethylsulfoxide-d_6): 1.84 μ_B/Cu. Solid state magnetic moment (MSB-Auto, 4.5 kG, 22.0 °C): 1.83 μ_B/Cu.

[CuL$^{1\text{-MeO}}$Na(CH$_3$OH)$_2$]ClO$_4$ (3c). $H_2L^{1\text{-MeO}}$ (0.044 g, 0.10 mmol) and $Cu(ClO_4)_2 \cdot 6H_2O$ (0.036 g, 0.10 mmol) were used (0.0480 g, 70% yield). Anal. Calcd for $C_{27}H_{37}ClCuN_3NaO_{10} \cdot H_2O$: C, 46.0, H, 5.6, N 6.0. Found: C, 45.3, H, 5.0, N, 6.6. UV/vis (CH_2Cl_2) [λ_{max}, nm (ε, M^{-1} cm^{-1})]: 283 (17,000), 342 (1,950), 423 (2,210) 594 (450 sh). FTIR (KBr): 2836 (s), 1595, 1569, 1481 (s), 1361, 1239, 1163, 1079, 960, 791, 747, 623 cm^{-1}. ESI-MS (MeOH): m/z = 521 $[CuL^{1\text{-MeO}} + Na]^+$. EPR (9.436 GHz, mod. amp. 5.0 G, CH_2Cl_2, 77 K): $g_\parallel$ = 2.295, $g_\perp$ = 2.086, and $A_\parallel$ = 176 G. Solution magnetic moment (Evans method, 19.8 °C, 5.50 × 10^{-3} M, acetonitrile-d_3): 1.59 μ_B. Solid state magnetic moment (MSB-Auto, 4.5 kG, 22.0 °C): 1.25 μ_B.

X-ray Crystal Structure Determination. X-ray quality crystals of **1a** and **1b** were obtained by ether diffusion into an acetonitrile or methanol solution of **1a** or **1b**, respectively. Single crystals of **2**, **3b**, and **3c** were obtained by slow evaporation of methanol solutions of the corresponding compounds, whereas X-ray quality crystals of **3a** were isolated by slow evaporation of a dichloromethane solution of **3a**. Intensity data for all complexes were collected using a diffractometer with a Bruker APEX ccd area detector.[13] Data were collected for all complexes except **3c** using graphite-monochromated Mo Kα radiation (λ = 0.71073 Å), while for **3c**, graphite-monochromated Cu Kα radiation (λ = 1.54178 Å) was used. The samples were cooled to 100(2) K. Cell parameters were determined from a nonlinear least-squares fit of the data. The data were corrected for absorption by the semiempirical method.[14] The structures were solved by direct methods and refined by full-matrix least-squares methods on F^2.[15] Hydrogen atom positions of hydrogens bonded to carbons were initially determined by geometry and refined by a riding model. Hydrogens bonded to nitrogens or oxygens were located on a difference map, and their positions were refined independently. Non-hydrogen atoms were refined with anisotropic displacement parameters. Hydrogen atom displacement parameters were set to 1.2 (1.5 for methyl) times the displacement parameters of the bonded atoms.

Table 1. Crystallographic Data for 1a, 1b, and 2

	1a·$2H_2O$	**1b**·$^1/_3CH_3CN$	**2**·CH_3OH·$^1/_2H_2O$
formula	$C_{46}H_{54}Cl_2Cu_3N_6O_6$	$C_{304}H_{330}Cl_{12}Cu_{18}N_{38}O_{72}$	$C_{41}H_{66}CuN_3O_{4.5}$
fw	1048.47	7237.18	736.51
crystal system	monoclinic	monoclinic	orthorhombic
space group	$C2/c$	$P2_1/c$	$P2_12_12_1$
a (Å)	19.352(3)	21.676(3)	12.597(2)
b (Å)	13.614(2)	43.659(6)	13.704(3)
c (Å)	19.977(3)	18.355(6)	23.683(5)
β (deg)	117.984	114.411(8)	90
V (Å^3)	4647.7(12)	15817(4)	4088.4(14)
Z	4	2	4
ρ_{calcd} mg/m^3	1.498	1.520	1.197
μ (mm^{-1})	1.529	1.368	0.579
θ (deg)	1.9 to 28.3	2.1 to 21.7	1.7 to 26.0
$R1$,[a] $wR2$[b] $[I > 2\sigma(I)]$	0.0431, 0.1231	0.0771, 0.2134	0.0273, 0.0769
GOF on F^2	1.001	1.044	1.020

[a] $R1 = \Sigma||F_{obs}| - |F_{calc}||/\Sigma|F_{obs}|$. [b] $wR2 = \{\Sigma[w(F_{obs}^2 - F_{calc}^2)^2]/\Sigma[w(F_{obs}^2)^2]\}^{1/2}$.

Complex **1a** was positioned on a crystallographic center of symmetry, and restraints on the water O−H bond lengths were required. For complex **1b**, the intensity data were truncated to 0.96 Å resolution because data in higher level shells all had $\langle I/\sigma \rangle < 2$. Four independent cationic trimers were found for complex **1b**, with two trimers located in general positions, and two trimers found to be near or on crystallographic centers of symmetry. The groups containing Cu7 and Cu9 were located near crystallographic centers of symmetry; thus, the occupancies of the atoms in these groups were set to 0.5. The Cu9 group is an example of "whole molecule" disorder. Most of the perchlorate groups were disordered with occupancies refined to 0.847(7) and 0.153(7) for N, 0.661(6) and 0.339(6) for O, 0.903(5) and 0.097(5) for P, 0.511(7) and 0.489(7) for Q, and, 0.592(7) and 0.408(7) for the R. The occupancies for the disordered Y acetonitrile refined to 0.544(11) and 0.456(11) for the unprimed and primed atoms. Restraints on the positional and displacement parameters of the disordered groups were required.

For complex **3a**, there are three metal complex molecules and two solvent (CH_2Cl_2) sites per asymmetric unit of the cell. Both solvent sites were severely disordered and were best modeled using the Squeeze program.[16] The N−H distances were restrained to be approximately equal. For complex **3b**, the intensity data were truncated to 0.94 Å resolution because data in higher resolution shells all had $R(\text{int}) > 0.25$. The second water site was so disordered that it was best modeled using the Squeeze program.[16] For complex **3c**, the perchlorate anion was disordered, and was modeled with refined occupancies of 0.591(8) and 0.409(8) for the A and B labeled groups. Restraints on the positional and displacement parameters of the perchlorate were required. Crystal data for all complexes are summarized in Tables 1 and 2. Selected bond lengths and angles for all complexes are summarized in Tables 3−8.

RESULTS

Syntheses and Structures. Ligands H_2L^1 and $H_2L^{1\text{-}tBu}$ were prepared by published procedures.[4a,9] All new ligands were synthesized in a similar manner by the Schiff base condensation of the precursor diamine, either ppda or phpda, with the appropriately substituted aldehyde followed by reduction with sodium borohydride to the diamine. The H_2L^1 family of ligands (H_2L^1, $H_2L^{1\text{-}tBu}$, $H_2L^{1\text{-}Br}$, $H_2L^{1\text{-}NO2}$, and $H_2L^{1\text{-}MeO}$, Scheme 1) differ from each other only in the substituents they have on their phenol rings. While the H_2L^1 ligand contains no substituents on the phenol ring, $H_2L^{1\text{-}tBu}$ and $H_2L^{1\text{-}Br}$ contain either *tert*-butyl or bromo substituents, respectively, in the 3- and 5-positions. $H_2L^{1\text{-}MeO}$ possesses a methoxy substituent in the 3-position, and $H_2L^{1\text{-}NO2}$ possesses a nitro substituent in the 5-position of the phenol ring. All five ligands contain the same potential N_3O_2 donor atom set, with pyridyl and amine N-donors, and, when deprotonated, phenolate O-donors. The diamine ligand H_2L^2 is different from the other five ligands in that it has a phenyl group instead of a pyridyl moiety, giving it a potential N_2O_2 donor atom set, with amine N-donors and, when deprotonated, phenolate O-donors (Scheme 1).

All new copper complexes were synthesized under an open air atmosphere by combining the copper salt, generally cupric chloride or cupric perchlorate, with the ligand and a base, either triethylamine or sodium hydride. The copper(II) complexes isolated in this study fall into two categories: either tricopper complexes similar to the previously reported $[\{CuL^1(CH_3CN)\}_2Cu](ClO_4)_2$ (**1**),[4a] namely, $[\{CuL^1Cl\}_2Cu]$ (**1a**) and $[\{CuL^2(CH_3CN)\}_2Cu](ClO_4)_2$ (**1b**), or monocopper complexes $[CuL^{1\text{-}tBu}(CH_3OH)]$ (**2**), $[CuL^{1\text{-}Br}]$ (**3a**), $[CuL^{1\text{-}NO2}]$ (**3b**), and $[CuL^{1\text{-}MeO}Na(CH_3OH)_2]ClO_4$ (**3c**). All six new copper complexes were characterized by elemental analysis, UV/visible spectroscopy, FTIR, EPR, solution and solid state magnetic susceptibility, and single crystal X-ray structural analysis.

Trinuclear complexes **1a** and **1b** are isostructural with the previously reported trinuclear complex **1** (Scheme 2).[4a] The difference between **1** and **1a** is simply in the counterion. The noncoordinating perchlorate anion in **1** leads to acetonitrile solvent molecules coordinating to two of the copper ions, while in **1a** the chloride anions coordinate (see Scheme 2). The difference between **1b** and the other two is in the ligand: **1b** was synthesized from H_2L^2 while **1** and **1a** were synthesized from H_2L^1. As mentioned above, H_2L^2 contains a phenyl group instead of a pyridyl group. However, this difference is inconsequential to the structures of **1** and **1b** since the pyridyl ring does not coordinate (vide infra), and they are isostructural, including the perchlorate counterions and the coordinated acetonitrile solvent molecules.

1, **1a**, and **1b** all contain three Cu^{2+} ions arranged in a linear array with two tetradentate ligands capping each end (Scheme 2 and Figure 1). The phenolato oxygen atoms of the ligands bridge to connect the terminal CuL^1 or CuL^2 units together via the third, central copper ion. The central copper(II) ion links the terminal units together via four μ_2-phenolato oxygen atoms of the two ligands in a square planar or nearly square planar environment. The τ_4 parameter, a measure of four coordinate geometry,[17] is zero for centrosymmetric **1a** and **1**,[4a] indicating perfect square planarity, while there is a slightly distorted square planar environment around the central copper in **1b**, with a τ_4 parameter of 0.09. The Cu−Cu distances in all three complexes are similar, ranging from 2.940 Å to 3.008 Å.

The terminal copper ions in all three complexes are five coordinate with slightly distorted square pyramidal geometries composed of N_2O_2 donor atoms from the ligand in the basal plane, and a coordinated chloride (**1a**) or acetonitrile (**1** and **1b**) ligand in the apical position. Similar to the τ_4 parameter, the τ_5 parameter is a measure of five-coordinate geometry.[18] The five-coordinate copper ions in complexes **1**, **1a**, and **1b** are all nearly

Table 2. Crystallographic Data for 3a−3c

	3a·$^2/_3CH_2Cl_2$	3b·$2H_2O$	3c
formula	$C_{71}H_{67}Br_{12}Cl_4Cu_3N_9O_6$	$C_{23}H_{27}CuN_5O_8$	$C_{27}H_{37}ClCuN_3NaO_{10}$
fw	2433.68	565.04	685.58
crystal system	monoclinic	orthorhombic	triclinic
space group	$P2_1/n$	$Pbca$	$P1$
a (Å)	13.626(5)	21.150(5)	10.6796(12)
b (Å)	20.992(8)	10.823(3)	11.1968(12)
c (Å)	29.684(12)	22.675(6)	15.2613(16)
α (deg)	90	90	99.326(8)
β (deg)	91.599(8)	90	104.157(8)
γ (deg)	90	90	114.830(9)
V (Å^3)	8487(6)	5190(2)	1531.5(3)
Z	4	8	2
ρ_{calcd} mg/m^3	1.905	1.446	1.487
μ (mm^{-1})	6.574	0.897	2.463
θ (deg)	1.9 to 25.3	2.0 to 25.3	3.1 to 67.1
$R1$,[a] $wR2$[b] $[I > 2\sigma(I)]$	0.0522, 0.1328	0.0747, 0.1935	0.0515, 0.1805
GOF on F^2	1.005	1.069	1.122

[a] $R1 = \Sigma||F_{obs}| - |F_{calc}||/\Sigma|F_{obs}|$. [b] $wR2 = \{\Sigma[w(F_{obs}^2 - F_{calc}^2)^2]/\Sigma[w(F_{obs}^2)^2]\}^{1/2}$.

Table 3. Selected Bond Lengths (Å) and Angles (deg) for 1a

Cu1−O1	1.9082(17)	Cu1−O28	1.9055(17)
Cu2−O1	1.9888(17)	Cu2−O28	1.9660(18)
Cu2−N9	1.986(2)	Cu2−N20	2.015(2)
Cu1−Cu2	2.9401(4)	Cu2−Cl1	2.5105(8)
O1−Cu2−O28A	100.26(7)	O28−Cu1−O1	79.74(7)
O1−Cu2−Cl1	91.74(6)	O28−Cu2−Cl1	93.97(6)
N20−Cu2−Cl1	99.80(7)	N9−Cu2−Cl1	98.47(7)
N9−Cu2−O1	91.58(8)	O28A−Cu2−O1	76.36(7)
O28−Cu2−N20	91.65(8)	N9−Cu2−N20	97.64(9)
O1−Cu2−N20	163.96(8)	O28−Cu2−N9	162.95(8)

perfectly square pyramidal, with τ_5 values of 0.0005,[4a] 0.017, and 0.053 for **1**, **1a**, and **1b**, respectively. The bond distances and angles for **1a** and **1b**, summarized in Tables 3 and 4, respectively, are very similar to each other and to complex **1**.[4a] Analogous to **1**, the perchlorate counterions in **1b** interact weakly with the terminal copper ions through the axial positions *trans* to the acetonitrile ligands. The pyridyl rings in **1** and **1a** do not coordinate to the copper ions, but instead are involved in intramolecular hydrogen bonding to one of the amine NH groups of the ligand (see Discussion section).

The solution behavior of **1a** and **1b** is essentially the same as that reported for **1**.[4a] All three species have very similar electronic spectra, with intense absorptions in the UV around 300 nm, medium intensity ($\varepsilon \sim 3000$ M^{-1} cm^{-1}) absorptions around 400 nm, and weak absorptions ($\varepsilon \sim 400$ M^{-1} cm^{-1}), presumably *d-d* transitions, around 600 nm. The EPR spectra of all three species are also very similar, with axial parameters typical for tetragonal copper complexes. The solution and solid state magnetic susceptibilities of all three complexes of around 1.1 μ_B/Cu are less than the spin-only value of 1.73 μ_B/Cu, suggesting some antiferromagnetic coupling. Previously we speculated that the axial EPR signal and lower than expected magnetic

Scheme 2

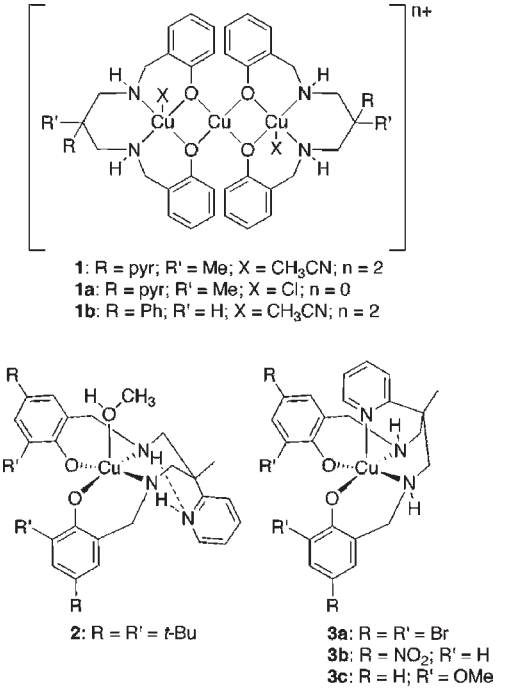

susceptibility for **1** was due to its dissociation into paramagnetic $[CuL^1]$ and antiferromagnetically coupled $[Cu_2L^1]^{2+}$ species.[4a] The only divergence in solution behavior between the new complexes, **1a** and **1b**, and **1** is in their electrospray ionization mass spectroscopy (ESI-MS). Unlike the ESI-MS of **1** where there was no evidence of the trimeric species in solution,[4a] prominent peaks in the ESI-MS of **1a** and **1b** suggest that they do not dissociate completely into monomeric species in solution. Complex **1a** displays a peak at $m/z = 974$ corresponding to $[Cu_3(L^1)_2Cl]^+$, and a peak at $m/z = 439$ corresponding to $[CuL^1 + H]^+$. Complex **1b** displays a prominent peak at $m/z = 455$ corresponding to $[Cu_3(L^2)_2]^{2+}$. However, these differences are not inconsistent with the hypothesis that all three trimers at least partially dissociate in solution into paramagnetic $[CuL^1]$ and antiferromagnetically coupled $[Cu_2L^1]^{2+}$ species.

Complexes **2** and **3a**−**c** are all mononuclear copper(II) complexes. In every case, the ligand coordinates to the copper(II) ion via the N_2O_2 donor atoms from the amine and phenolate groups of the doubly deprotonated ligands. The difference between complex **2** and the other mononuclear complexes **3a**−**c** is that the pyridyl group does not coordinate in **2**, while it does coordinate in **3a**−**c**. The X-ray structure of **2** revealed that it consists of a five coordinate copper(II) ion in an approximately square pyramidal geometry ($\tau_5 = 0.095$), with a solvent methanol ligand occupying the apical position (Figure 2). The N_2O_2 donor set from $(L^{1\text{-}t\text{Bu}})^{2-}$ occupies the basal plane of the pyramid. The bond distances and angles, summarized in Table 5, are typical of square pyramidal copper(II) complexes with similar ligands, and the apical Cu−O_{MeOH} bond is, not surprisingly, longer than the bonds in the basal plane. Similar to **1** and **1a**, the pyridyl N atom of the ligand in **2** does not coordinate to the metal center, but instead is involved with hydrogen bonding between the pyridyl N atom and the amine NH groups. The six-membered chelate ring made up of the copper, nitrogen, and propylene carbon atoms of the ligand adopts the chair conformation, and the amine NH

dx.doi.org/10.1021/ic201536c |*Inorg. Chem.* 2011, 50, 11581–11591

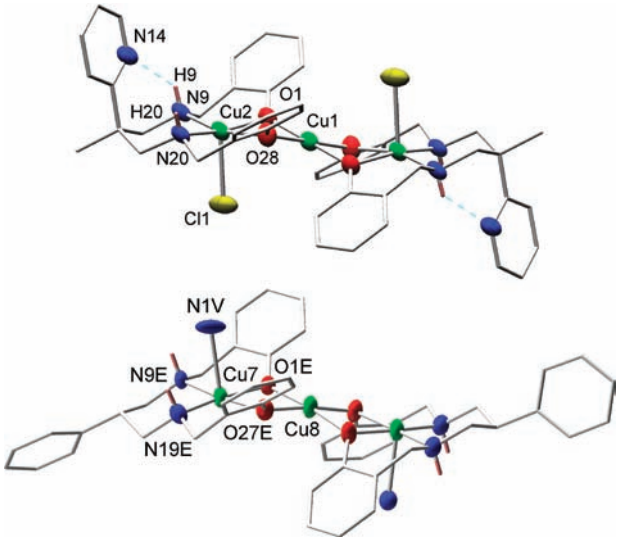

Figure 1. Representations of the X-ray structures of **1a** (top) and **1b** (bottom). All H atoms except for the amine protons have been removed for clarity. For **1b**, one of the four crystallographically independent copper trimers is shown, only the N atom of the coordinated CH_3CN molecules are shown for clarity, and the perchlorate anions are also omitted for clarity.

Table 4. Selected Bond Lengths (Å) and Angles (deg) for One of the Crystallographically Independent Copper Trimers in 1b[a]

Cu7−O1E	1.970(10)	Cu7−O27E	1.945(12)
Cu7−N9E	1.956(14)	Cu7−N19E	2.021(12)
Cu7−N 1 V	2.457(12)	Cu2−O1E	1.896(12)
Cu2−O27E	1.943(9)	Cu7−Cu8	2.980(14)
O1E−Cu7−N9E	95.7(5)	O27E−Cu7−N19E	92.3(6)
O27E−Cu7−O1E	77.9(5)	N19E−Cu7−N 1 V	87.0(4)
N9E−Cu7−N19E	94.0(6)	N9E−Cu7−N 1 V	91.4(4)
O27E−Cu7−N 1 V	90.8(4)	O1E−Cu7−N19E	170.2(6)
O1E−Cu7−N 1 V	92.7(4)	O1E−Cu8−O27E	79.8(5)
O27E′−Cu8−O1E	100.2(5)	O27E−Cu7−N9E	173.4(5)
O1E′−Cu8−O1E	179.995(2)	O27E−Cu8−O27E′	180.0(8)

[a] Listings of the bond distances and and angles for the other trimer molecules in **1b** can be found in the Supporting Information.

bonds are on the apical side of copper's square pyramidal coordination sphere. The phenolate rings are canted on either side of the basal plane of the copper coordination sphere. One *tert*-butyl substituted ring lies above the plane, in closer proximity to the coordinated methanol ligand, while the other ring lies below the plane.

Complexes **3a**−**c** all contain a five-coordinate copper(II) ion with slightly distorted square pyramidal geometries, having τ_5 values of 0.097, 0.00083, and 0.0053, respectively. In contrast to **1**, **1a**, or **2**, the copper(II) ions in **3a**−**c** are coordinated with N_3O_2 donor atom sets that include two amine N atoms and two deprotonated O, and, importantly, also the pyridyl N atom (Figures 3−5). The amine N and phenolate O atoms occupy the basal plane and the pyridyl N atom occupies the apical position of the square pyramid. Whereas the six-membered chelate ring made up of the copper, nitrogen, and carbon atoms in complexes **1**, **1a**, **1b**, and **2** all adopted the chair conformation, in **3a**−**c** the chelate ring is in the boat form. Additionally, the

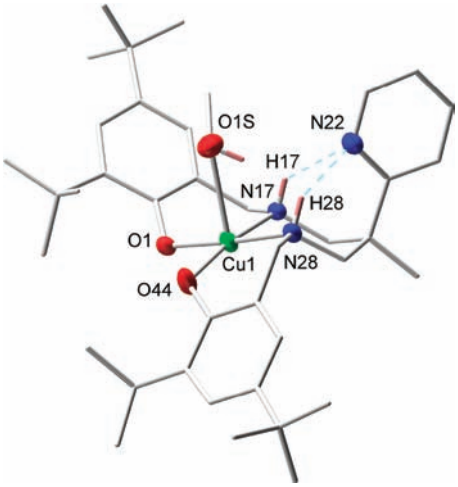

Figure 2. Representation of the X-ray structure of **2**. All H atoms except for the amine and CH_3OH protons have been removed for clarity.

Table 5. Selected Bond Lengths (Å) and Angles (deg) for 2

Cu1−O1	1.9467(12)	Cu1−O44	1.9182(13)
Cu1−N17	2.0328(14)	Cu1−N28	2.0226(15)
Cu1−O1S	2.5287(14)		
O1−Cu1−N17	92.25(5)	N28−Cu1−N17	87.65(6)
O44−Cu1−O1	88.02(5)	O44−Cu1−N28	92.61(6)
O1−Cu1−N28	176.56(6)	O44−Cu1−N17	170.94(6)

amine NH groups in **3a**−**c** are on the opposite side of the apical coordination site. These structural features are related to the coordination of the pyridyl ring to the copper, and will be examined in detail in the Discussion section.

The solid state structure of **3a** contains three symmetry-related subunits of $[CuL^{1\text{-Br}}]$ connected by intermolecular hydrogen bonding (Figure 3, bottom). Both NH groups in each complex are hydrogen bonded to a phenoxo O atom of an adjacent complex, forming a C_3 symmetric supramolecular trimer held together by a total of six NH···O hydrogen bonds. Perhaps as a consequence of the steric hindrance introduced by the intermolecular H-bonds, the phenolate rings of the $(L^{1\text{-Br}})^{2-}$ ligands are folded above the CuN_2O_2 basal plane of the square pyramid in **3a**. This stands in contrast to isostructural **3b** and **3c**, which have the phenolate rings canted above and below the basal plane in each complex (Figures 4 and 5).

Attempts to synthesize copper(II) complexes with $H_2L^{1\text{-MeO}}$ using triethylamine as the base for phenol deprotonation were unsuccessful, but using NaH as the base resulted in the heterometallic binuclear copper/sodium complex $[CuL^{1\text{-MeO}}Na(CH_3OH)_2]ClO_4$ (**3c**). As mentioned above, the coordination sphere around the copper ion is isostructural with **3a** and **3b**. The six-coordinate sodium ion is chelated by the phenolate and methoxy O atoms from both phenol rings, plus two coordinated CH_3OH ligands, forming a distorted octahedral geometry. The phenolate O atoms bridge between the copper and sodium ions such that the methanol ligands are *trans* to each other. The ESI-MS of **3c** suggests that the heterometallic complex is at least partially present in solution, since a peak at m/z = 521 corresponding to $[CuL^{1\text{-MeO}} + Na]^+$ was observed.

Cyclic Voltammetry. The electrochemical behavior of all six complexes was studied by cyclic voltammetry in acetonitrile

dx.doi.org/10.1021/ic201536c |*Inorg. Chem.* 2011, 50, 11581–11591

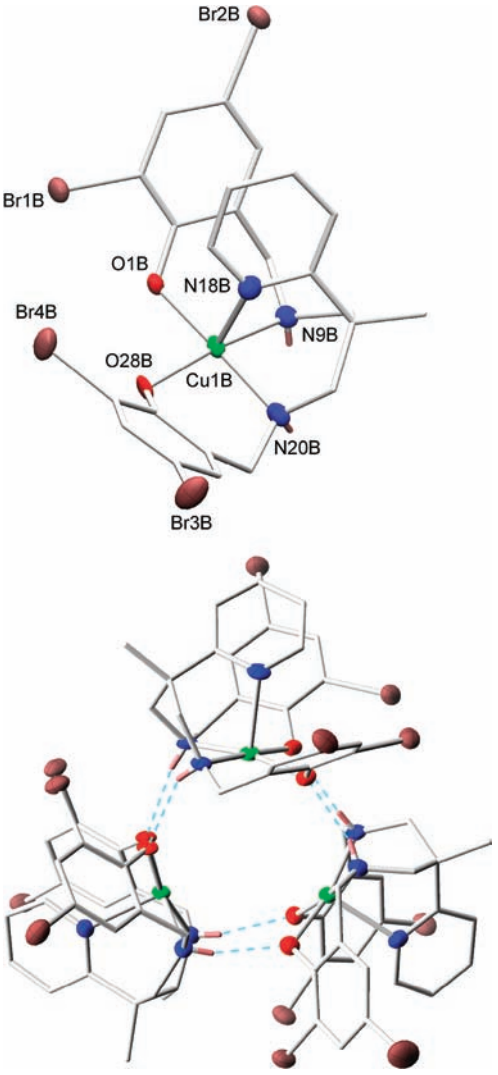

Figure 3. Representation of the X-ray structure of **3a** (top), and the intermolecular H-bonding interactions in the trimeric units of **3a** (bottom). All H atoms except for the amine protons have been removed for clarity.

(**1**, **1b**, **2**, **3a**, and **3b**), dichloromethane (**1a**, **2**, and **3c**), or DMF (**3a**). In some cases, it was not possible because of poor solubility to obtain cyclic voltammograms (CVs) in the same solvent. For example, **1a** was only soluble enough in dichloromethane to obtain electrochemical data, while for **3a** the CV in acetonitrile had a very large ΔE but much a smaller ΔE in DMF. Interestingly, the redox behavior of **2** was very solvent dependent, displaying a well behaved Cu^{II}/Cu^{I} redox couple in acetonitrile, while in dichloromethane having no metal-centered redox activity (vide infra).

The CVs of all six complexes (Figure 6) showed quasi-reversible Cu^{II}/Cu^{I} redox waves at potentials ranging from −680 mV to −1055 mV versus Ag/AgCl (Supporting Information, Figures S1−S6, and Table 9). As can be observed in Table 9, the half-wave potentials ($E_{1/2}$) of complexes **1**, **1a**, **2**, and **3a**−**c** become decreasingly less negative as the ligand becomes more electron-withdrawing: $H_2L^{1\text{-}tBu} < H_2L^{1} \approx H_2L^{1\text{-}MeO} < H_2L^{1\text{-}Br} < H_2L^{1\text{-}NO2}$. The influence of the substituents present on the phenol rings of the ligands on the Cu^{II}/Cu^{I} redox couple is

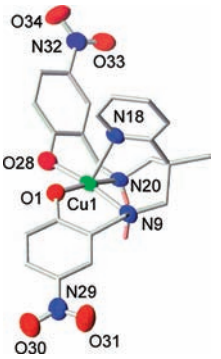

Figure 4. Representation of X-ray structure of **3b** with all H atoms except for amine protons removed for clarity.

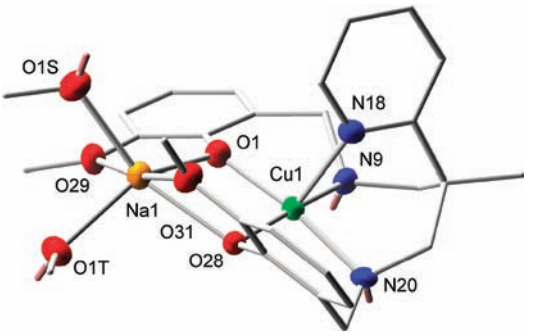

Figure 5. Representation of X-ray structure of **3c** with all H atoms except for amine protons removed for clarity.

Table 6. Selected Bond Lengths (Å) and Angles (deg) for One Independent Molecule of 3a

Cu1B−O1B	1.942(5)	Cu1B−O28B	1.951(4)
Cu1B−N9B	2.046(6)	Cu1B−N20B	1.996(6)
Cu1B−N18B	2.325(5)		
O1B−Cu1B−O28B	89.44(19)	N20B−Cu1B−N9B	84.3(2)
O1B−Cu1B−N20B	174.5(2)	O1B−Cu1B−N18B	95.40(19)
O28B−Cu1B−N20B	93.5(2)	O28B−Cu1B−N18B	93.80(19)
O1B−Cu1B−N9B	91.9(2)	N20B−Cu1B−N18B	89.0(2)
O28B−Cu1B−N9B	168.72(19)	N9B−Cu1B−N18B	97.2(2)

clearly indicated by the increasingly negative $E_{1/2}$ values. The electron-withdrawing bromo- and nitro-groups in **3a** and **3b**, respectively, lead to less negative half-wave potentials of −897 mV and −680 mV versus Ag/AgCl in acetonitrile. The $E_{1/2}$ of −713 mV versus Ag/AgCl for **3a** in DMF is slightly less than in acetonitrile, and ΔE is significantly smaller for **3a** in DMF. The more electron donating *tert*-butyl groups on the ligand in **2** lead to the largest negative $E_{1/2}$ of −1055 mV versus Ag/AgCl. The redox potential for **1b**, which contains the $(L^2)^{2-}$ ligand, is similar to the $E_{1/2}$ for **1**, which is not surprising since they are, with the exception of the pyridyl ring, isostructural.

The electrochemical behavior of **2** in dichloromethane differs significantly from **2** in acetonitrile. While the $E_{1/2}$ for **2** in acetonitrile is −1055 mV versus Ag/AgCl, no metal-centered redox wave was observed for **2** in dichloromethane from 0 to −1800 mV at all scan rates. This phenomena was also observed in the oxo-bridged diiron complex of the same ligand, $[(FeL^{1\text{-}tBu})_2(\mu\text{-}O]$.[9]

dx.doi.org/10.1021/ic201536c |*Inorg. Chem.* 2011, 50, 11581–11591

Table 7. Selected Bond Lengths (Å) and Angles (deg) for 3b

Cu1−O1	1.935(4)	Cu1−O28	1.976(4)
Cu1−N9	2.062(5)	Cu1−N20	1.995(5)
Cu1−N18	2.226(4)		
O1−Cu1−O28	84.65(16)	N20−Cu1−N9	87.82(19)
O1−Cu1−N20	171.51(18)	O1−Cu1−N18	98.66(17)
O28−Cu1−N20	92.97(19)	O28−Cu1−N18	100.63(17)
O1−Cu1−N9	93.31(17)	N20−Cu1−N18	89.78(18)
O28−Cu1−N9	171.33(18)	N9−Cu1−N18	88.00(18)

Table 8. Selected Bond Lengths (Å) and Angles (deg) for 3c

Cu1−O1	1.950(3)	Cu1−O28	1.923(3)
Cu1−N9	2.028(4)	Cu1−N20	2.041(4)
Cu1−N18	2.246(4)		
O28−Cu1−O1	84.46(14)	O1−Cu1−N18	101.12(14)
O1−Cu1−N9	92.70(16)	O28−Cu1−N20	92.90(15)
N9−Cu1−N20	88.50(17)	N9−Cu1−N18	90.10(16)
O28−Cu1−N18	98.94(14)	N20−Cu1−N18	88.24(15)
O28−Cu1−N9	170.88(16)	O1−Cu1−N20	170.56(15)

However, **2** in dichloromethane exhibits two quasi-reversible one-electron redox couples at 579 mV (ΔE = 179 mV) and 1022 mV (ΔE = 108 mV), versus Ag/AgCl. These features are attributed to the oxidation of the *tert*-butyl substituted phenolate groups leading to the formation of phenoxyl radicals. These ligand-based redox features for **2** in acetonitrile appear as irreversible oxidations. None of the other complexes in this study displayed any of this type of ligand-centered redox process, which is typically seen for complexes with *tert*-butyl substituted salen-type ligands.[8a,d,20]

The substituent effects on the redox potentials of **1**, **1a**, **2**, and **3a**−**c** were analyzed by Hammett analysis. A plot of $E_{1/2}$ versus Hammett σ_p parameter[19] for the reduction of Cu(II) center is shown in Figure 7. Since the CVs of all complexes were not possible in acetonitrile, the Hammett analysis is most relevant for complexes **1**, **2**, **3a**, and **3b** (represented by squares in Figure 7). The data for **1a** and **3c** in dichloromethane (triangles in Figure 7) are included to illustrate the similar redox potentials in that solvent; however, a direct comparison in the Hammett analysis is not warranted because of solvent dependent differences in redox potentials. Furthermore, it is important to point out that the Hammett analysis compares the $E_{1/2}$ with the Hammett parameter for the *para*-position, σ_p. The *ortho*-substitution of the methoxy groups in $HL^{1\text{-MeO}}$ does not affect σ_p, and indeed the σ_p value used **3c** is the same as for the complexes with H-substituted para positions in their ligands.

A linear relationship for $E_{1/2}$ versus σ_p is obtained for these complexes, with a calculated slope of 382 mV. The Hammett plot supports the electronic effects that the substituents on the H_2L^1 family of ligands have on the redox potentials of their copper complexes. The more electron-rich copper centers in **1**, **1a**, and **2** have larger negative potentials and are hence more difficult to reduce, while the electron deficient copper centers in **3a** and **3b** have relatively smaller negative potentials and are thus easier to reduce. These electronic effects are also key to understanding the structural differences in these complexes.

DISCUSSION

The complexes in this study synthesized with the H_2L^1 family of ligands have the pyridyl group either coordinated to the copper center (**3a**−**c**) or not coordinated and involved in hydrogen bonding (**1**, **1a**, and **2**). Similar complexes with pyridyl-containing ligands have shown this same phenomenon of the pyridyl ring not coordinating: for example, $[CuL^{imine}(CH_3CN)\}]$,[4a] and a series of copper(II) complexes with a related pyridylbis(guanidine) ligand.[4b] In these species, the sp^2 hybridization of the N atoms in the imine and guanidine ligands result in a more planar six-membered chelate ring, leading to the inability of the pyridyl ring to coordinate to the copper atom. However, in the case of complexes of the diamine ligands, the explanation is not as simple.

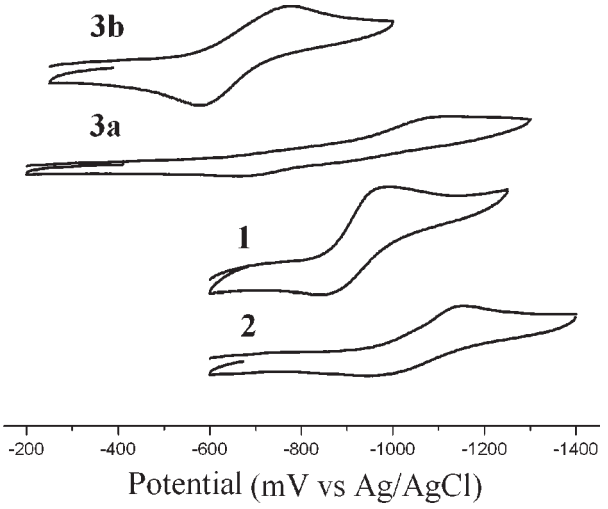

Figure 6. CVs of the complexes with the H_2L^1 family of ligands soluble in acetonitrile: **1**, **2**, **3a**, and **3b** in CH_3CN containing 0.1 M $TBAPF_6$ and at a scan rate of 100 mV/s.

The ligands studied in this paper (i.e., H_2L^1 and its derivatives plus H_2L^2) have in common the 1,3-propanediamine backbone attached to the methylenephenol groups. The 2-position of the propyl backbone contains either the pyridyl group (H_2L^1 family of ligands) or the phenyl group (H_2L^2). When the prochiral amine groups coordinate to a metal center, they lock in either the *R* or *S* conformation on each amine. The possible metal complex isomers include the *R*,*R* and *S*,*S* enantiomeric pair, and the *meso*-(*s*) and *meso*-(*r*) diastereomers (Scheme 3). The *meso* isomers impose pseudochirality on the 2-position of the propyl backbone, giving rise to the two diastereomers. Because of the rapid pyramidal inversion of the secondary amines in solution prior to coordination,[21] presumably all isomers can be accessed, but only the most thermodynamically stable conformations will prevail.

The six-membered chelate ring that is formed when the ligand coordinates to a metal ion can adopt either a chair or boat conformation. All of the structures reported in this paper have the ligand coordinated in either the *meso*-(*s*) or the *meso*-(*r*) conformation, and in every case the amine H atoms are in axial positions on the cyclohexane-like ring, as illustrated in Scheme 3. Scheme 3 shows the two *meso* diastereomers in the chair conformation on the left and the boat conformation on the right. The key difference between the *meso*-(*s*) and *meso*-(*r*) diastereomers can be seen when comparing them in the chair conformation: in the case of *meso*-(*s*)-chair the methyl group is axial while the *meso*-(*r*)-chair has the pyridyl group in the axial position.

The preferred conformations of the *meso*-(*s*) or *meso*-(*r*) diastereomers, highlighted in boxes in Scheme 3, can now be seen.

Table 9. Electrochemical Data for 1, 1a−b, 2, and 3a−c

complex[a]	solvent	$E_{1/2}$ (mV) [b]	ΔE (mV)	σ_p [c]	reference
$[\{CuL^1(CH_3CN)\}_2Cu](ClO_4)_2$ (**1**)	CH_3CN	−914	139	0	4a
$[\{CuL^1Cl\}_2Cu]$ (**1a**)	CH_2Cl_2	−1040	260	0	this work
$[\{CuL^2(CH_3CN)\}_2Cu](ClO_4)_2$ (**1b**)	CH_3CN	−875	170	0	this work
$[CuL^{1\text{-}tBu}(CH_3OH)]$ (**2**)	CH_3CN	−1055	199	−0.2	this work
	CH_2Cl_2	579	179		this work
	CH_2Cl_2	1022	108		this work
$[CuL^{1\text{-}Br}]$ (**3a**)	CH_3CN	−897	430	0.23	this work
	DMF	−713	232		this work
$[CuL^{1\text{-}NO2}]$ (**3b**)	CH_3CN	−680	210	0.78	this work
$[CuL^{1\text{-}MeO}Na(CH_3OH)_2]ClO_4$ (**3c**)	CH_2Cl_2	−954	367	0	this work

[a] Sample concentrations were all approximately 1.0 mM. [b] Scan rate = 100 mV s^{-1}; 0.1 M $TBAPF_6$ supporting electrolyte. [c] Values obtained from ref 19.

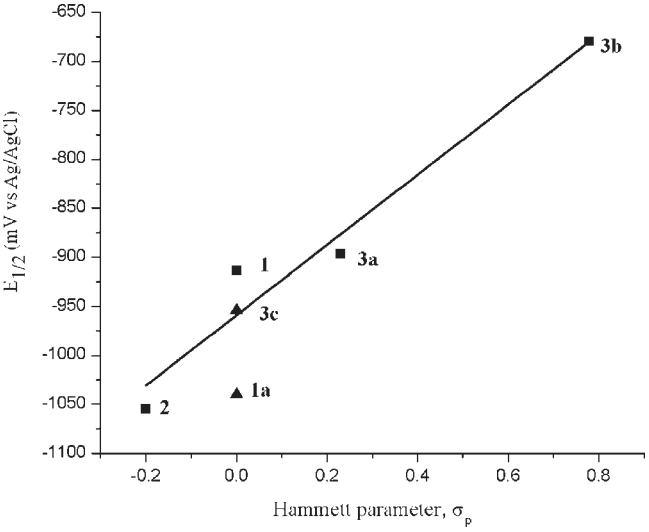

Figure 7. Plot of $E_{1/2}$ vs the Hammett σ_p parameter for compounds **1**, **1a**, **2**, and **3a**−**c** in CH_3CN (■) or CH_2Cl_2 (▲).

Scheme 3

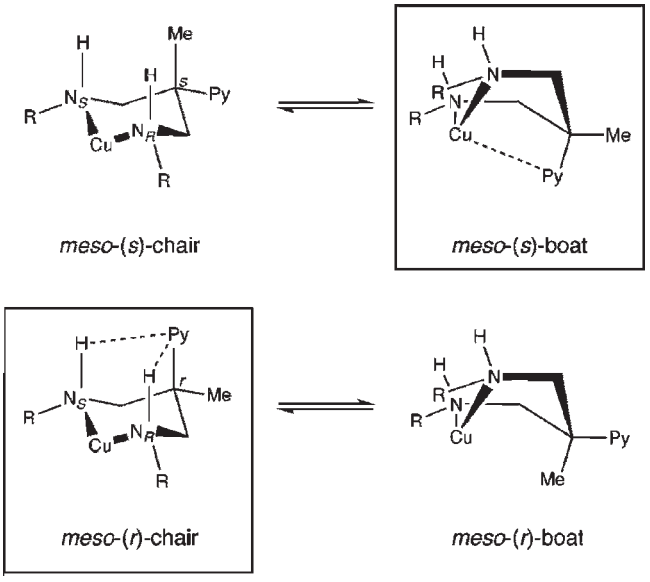

The *meso*-(*s*)-boat conformation places the pyridyl group within coordination distance of the copper ion, allowing for pentadentate coordination by the ligand. The chair form of the same diastereomer, that is, *meso*-(*s*), would be less favorable, since no intramolecular coordinate or hydrogen bonds involving the pyridyl ring are possible. Conversely, it is not possible to coordinate the pyridyl ring to the metal center in the *meso*-(*r*) diastereomer. While the *meso*-(*r*)-chair form places the pyridyl ring in proximity of the NH groups, allowing hydrogen bonding, it is too far away from the copper center to coordinate. Folding the *meso*-(*r*) diastereomer into the boat form moves the pyridyl ring even farther away from the copper, and eliminates the possibility of hydrogen bonding with the amine NH groups. Therefore, the *meso*-(*s*)-boat and the *meso*-(*r*)-chair conformations (Scheme 3, in boxes) are the two most stable structures possible for these ligands. This conclusion is borne out in the structures of the complexes reported in this study.

The tricopper complexes (**1**, **1a**, and **1b**) are all composed of two five-coordinate copper(II) species linked via bridging phenolate O-atoms to a third, four-coordinate copper ion (Scheme 2 and Figure 1). The ligands coordinate through the two amine N-atoms and two phenolate O-atoms in the basal plane of the nearly perfect square pyramids of the terminal copper ions. The axial positions of the square pyramids are occupied by CH_3CN solvent ligands (**1** and **1b**) or chloride ligands (**1a**). The pyridyl rings of the ligands in **1** and **1a** do not coordinate to the Cu ions. The pyridyl ring N atoms in **1** and **1a** are involved in hydrogen bonding to one of the amine NH groups of the same ligand (see Figure 1), adopting the *meso*-(*r*)-chair conformation. Although ligand H_2L^2 does not contain the pyridyl group, the structure of **1b** is very similar to those of **1** and **1a**, with the exception of the H-bonding to the amine NH groups. Likewise, in mononuclear, square pyramidal complex **2** with ligand $H_2L^{1\text{-}tBu}$, the pyridyl ring does not coordinate and instead forms hydrogen bonds with both amine NH groups in the *meso*-(*r*)-chair conformation.

In contrast, complexes **3a**−**c** all contain the ligand coordinated to the copper ion in the *meso*-(*s*)-boat conformation with the pyridyl ring coordinating. The coordination spheres in the equatorial planes of the square pyramidal copper centers in **3a**−**c** are also made up of the two N-atoms and two O-atoms from the amine and phenolate groups of the ligands. One consequence of the *meso*-(*s*)-boat coordination mode is that the amine NH groups are now no longer involved in intramolecular hydrogen bonding with the pyridyl ring. In the case of **3a**, this allows for intermolecular hydrogen bonding to

dx.doi.org/10.1021/ic201536c |*Inorg. Chem.* 2011, 50, 11581–11591

occur which leads to the H-bonded cyclic trimers seen in its solid state structure (see Figure 3, bottom).

The reason why the *meso*-(*r*)-chair coordination mode is chosen in some cases (**1**, **1a**−**b**, and **2**) while the *meso*-(*s*)-boat coordination mode is chosen in others (**3a**−**c**) can be rationalized on the basis of the electronic properties of the ligands. The nucleophilicity of the phenolato oxygens on the ligands correlate with the electron donating or withdrawing nature of the substituents in the position para to the OH group on the phenol rings, and these can be quantified in a qualitative way by their Hammett σ_p parameters, tabulated in Table 9.[19] The Hammett σ_p parameters and nucleophilicity of the phenolate oxygens of the ligands increase in the following order: $H_2L^{1\text{-}NO2}$ < $H_2L^{1\text{-}Br}$ < H_2L^{1} ≈ $H_2L^{1\text{-}MeO}$ < $H_2L^{1\text{-}t\text{Bu}}$. Several of the ligands ($H_2L^{1\text{-}t\text{Bu}}$, $H_2L^{1\text{-}MeO}$, and $H_2L^{1\text{-}Br}$) have substituents in the ortho positions relative to the phenol OH group, but this is of minor consequence to the nucleophilicity of the phenolato oxygen. The nucleophilicity of the ligands correlates nicely with the electrochemical potentials of the Cu(I)/Cu(II) couples (Figure 7).

The possibility that steric factors influence the determination of *meso*-(*r*)-chair or *meso*-(*s*)-boat coordination mode has been considered as well. The most sterically hindered ligand, the *tert*-butyl substituted $H_2L^{1\text{-}t\text{Bu}}$, coordinates to copper in the *meso*-(*r*)-chair mode in **2**, suggesting that the bulky *tert*-butyl groups in the 2-positions of the phelolate rings might interfere with the ability of the pyridyl ring to coordinate to the copper in the *meso*-(*s*)-boat coordination mode. However, inspection of the structure of **2** reveals that the phenolate rings are disposed on opposite sides of the basal plane of the copper coordination sphere, and potential interactions between the 2-position *tert*-butyl group on the side of the basal plane that would accept the pyridyl group in the *meso*-(*s*)-boat mode would be longer than 3 Å. The argument that the ligand coordination geometry where the phenolate rings are disposed on either side of the basal plane might impose geometric constraints that prevent the *meso*-(*s*)-boat coordination mode is weakened by the fact that this very example is observed in complex **3b**. The phenolate groups in **3b** are canted above and below the copper basal plane, but the complex adopts the *meso*-(*s*)-boat coordination mode with the pyridyl ring coordinated to the copper. Finally, the unsubstituted ligand H_2L^1, where the least amount of steric hindrance would be expected, coordinates in the *meso*-(*r*)-chair mode in **1** and **1a**, suggesting an alternate explanation for the coordination preferences of the ligand.

The complexes with the *meso*-(*r*)-chair coordination mode (**1**, **1a**−**b**, and **2**) contain the more nucleophilic phenolato groups in ligands $H_2L^{1\text{-}t\text{Bu}}$ and H_2L^1, while the complexes with the *meso*-(*s*)-boat coordination mode (**3a**−**c**) have, in the cases of $H_2L^{1\text{-}Br}$ and $H_2L^{1\text{-}NO2}$, less nucleophilic phenolate oxygens because of the electron withdrawing nature of Br and NO_2. We surmise that the less nucleophilic phenolato donors ($H_2L^{1\text{-}Br}$ and $H_2L^{1\text{-}NO2}$) leave the copper ion somewhat electron deficient, making the coordination of the pyridyl ring more favorable and leading to the *meso*-(*s*)-boat coordination mode. In the case of the more nucleophilic donors ($H_2L^{1\text{-}t\text{Bu}}$ and H_2L^1), the copper center has more electron density and hence there is less energetic benefit from the coordination of the pyridyl ring than is gained from hydrogen bonding between the pyridyl ring and the amine NH groups. The case of complex **3c**, which also has the *meso*-(*s*)-boat coordination mode, is noteworthy in that its $H_2L^{1\text{-}MeO}$ ligand's phenolato oxygen nucleophilicity is expected to be close to that of H_2L^1, yet it has the *meso*-(*s*)-boat coordination mode. This may be partially due to the coordination of the methoxy substituents to the sodium ion in **3c**, which may draw electron density away from the copper center and therefore favor the coordination of the pyridyl group in the *meso*-(*s*)-boat coordination mode.

■ ASSOCIATED CONTENT

Supporting Information. X-ray structural information (CIF) and CVs for **1a**, **1b**, **2**, and **3a**−**3c**. This material is available free of charge via the Internet at http://pubs.acs.org.

■ AUTHOR INFORMATION

Corresponding Author

*E-mail: houser@ou.edu.

Present Addresses

[†]Department of Chemistry, Wayne State University, 5101 Cass Ave, Detroit, MI 48202.

■ ACKNOWLEDGMENT

This work was supported by the National Science Foundation (NSF CHE-0616941) and the University of Oklahoma. Additionally, we thank the NSF for the purchase of a CCD-equipped X-ray diffractometer (CHE-0130835).

■ REFERENCES

(1) Fenton, H.; Tidmarsh, I. S.; Ward, M. D. *Dalton Trans.* **2009**, 4199.

(2) *Nomenclature of inorganic chemistry IUPAC recommendations 2005*; RSC Publishing: Cambridge, U.K., 2005.

(3) Kirin, S. I.; Happel, C. M.; Hrubanova, S.; Weyhermuller, T.; Klein, C.; Metzler-Nolte, N. *Dalton Trans.* **2004**, 1201.

(4) (a) Shakya, R.; Jozwiuk, A.; Powell, D. R.; Houser, R. P. *Inorg. Chem.* **2009**, *48*, 4083. (b) Pal Chaudhuri, U.; Powell, D. R.; Houser, R. P. *Inorg. Chim. Acta* **2009**, *362*, 2371.

(5) Malassa, A.; Gorls, H.; Buchholz, A.; Plass, W.; Westerhausen, M. Z. *Anorg. Allg. Chem.* **2006**, *632*, 2355.

(6) Doro, F. G.; Castellano, E. E.; Moraes, L. A. B.; Eberlin, M. N.; Tfouni, E. *Inorg. Chem.* **2008**, *47*, 4118.

(7) Yang, L.; Powell, D. R.; Klein, E. L.; Grohmann, A.; Houser, R. P. *Inorg. Chem.* **2007**, *46*, 6831.

(8) (a) Mukherjee, C.; Weyhermuller, T.; Bothe, E.; Chaudhuri, P. *Inorg. Chem.* **2008**, *47*, 11620. (b) Roy, N.; Sproules, S.; Bothe, E.; Weyhermuller, T.; Wieghardt, K. *Eur. J. Inorg. Chem.* **2009**, 2655. (c) Orio, M.; Jarjayes, O.; Kanso, H.; Philouze, C.; Neese, F.; Thomas, F. *Angew. Chem., Int. Ed.* **2010**, *49*, 4989. (d) Storr, T.; Verma, P.; Pratt, R. C.; Wasinger, E. C.; Shimazaki, Y.; Stack, T. D. P. *J. Am. Chem. Soc.* **2008**, *130*, 15448. (e) Whittaker, J. W. *Chem. Rev.* **2003**, *103*, 2347. (f) Rolff, M.; Schottenheim, J.; Decker, H.; Tuczek, F. *Chem. Soc. Rev.* **2011**, *40*, 4077. (g) Benisvy, L.; Wanke, R.; da Silva, M.; Pombeiro, A. J. L. *Eur. J. Inorg. Chem.* **2011**, 2791. (h) Arora, H.; Philouze, C.; Jarjayes, O.; Thomas, F. *Dalton Trans.* **2010**, *39*, 10088.

(9) Shakya, R.; Powell, D. R.; Houser, R. P. *Eur. J. Inorg. Chem.* **2009**, 5319.

(10) Friedrich, S.; Schubart, M.; Gade, L. H.; Scowen, I. J.; Edwards, A. J.; McPartlin, M. *Chem. Ber./Recl.* **1997**, *130*, 1751.

(11) Busto, E.; Gotor-Fernandez, V.; Montejo-Bernardo, J.; Garcia-Granda, S.; Gotor, V. *Org. Lett.* **2007**, *9*, 4203.

(12) Evans, D. F. *J. Chem. Soc.* **1959**, 2003.

(13) (a) *SMART Software Reference Manual*; Bruker-AXS: Madison, WI, 1998; (b) *SAINT Software Reference Manual*; Bruker-AXS: Madison, WI, 1998.

(14) Sheldrick, G. M. *SADABS, Program for empirical absorption correction of area detector data*; University of Göttingen: Göttingen, Germany, 2002.
(15) (a) Sheldrick, G. M. *SHELXTL Version 6.10 Reference Manual*; Bruker AXS Inc.: Madison, WI, 2000; (b) *International Tables for Crystallography*; Kluwer: Boston, MA, 1995; Vol. C.
(16) van der Sluis, P.; Spek, A. L. *Acta Crystallogr., Sect. A* **1990**, *A46*, 194.
(17) Yang, L.; Powell, D. R.; Houser, R. P. *Dalton Trans.* **2007**, 955.
(18) Addison, A. W.; Rao, T. N.; Reedijk, J.; van Rijn, J.; Verschoor, G. C. *J. Chem. Soc., Dalton Trans.* **1984**, 1349.
(19) Hansch, C.; Leo, A.; Taft, R. W. *Chem. Rev.* **1991**, *91*, 165.
(20) (a) Benisvy, L.; Blake, A. J.; Collison, D.; Davies, E. S.; Garner, C. D.; McInnes, E. J. L.; McMaster, J.; Whittaker, G.; Wilson, C. *Dalton Trans.* **2003**, 1975. (b) Maki, T.; Araki, Y.; Ishida, Y.; Onomura, O.; Matsumura, Y. *J. Am. Chem. Soc.* **2001**, *123*, 3371.
(21) Rauk, A.; Allen, L. C.; Mislow, K. *Angew. Chem., Int. Ed.* **1970**, *9*, 400.